16th World Conference on Earthquake, 16WCEE 2017
Santiago Chile, January 9th to 13th 2017
Paper N° 2406
Registration Code: S-K1464707919

Implementation of Elastomeric Seismic Isolation in Tall Buildings Considering Axial-Lateral Coupling in the Isolators

Nelson Maureira[(1)], Juan C. de la Llera[(2)]

[(1)] Lecturer, Universidad Católica de la Santísima Concepción, Concepción- Chile, nmaureira@ucsc.cl
[(2)] Principal Researcher, National Center for the Integrated Management of Natural Disasters (CIGIDEN), CONICYT/FONDAP/15110017, Facultad de Ingeniería, Pontificia Universidad Católica de Chile, e-mail: jcllera@ing.puc.cl

Abstract

Seismic isolation of high-rise buildings presents an opportunity but also a challenge to seismic isolation, a technique mostly used in the past in low and moderate-rise buildings. It turns out that under certain conditions of the structure and input, it is perfectly reasonable to protect tall structures using seismic isolation. The objective of this research is to explore these conditions in simple structural models. A parametric analysis on seismically isolated tall buildings was performed using first a simplified representation of the superstructure as a 3D rigid rectangular prism, geometrically characterized by its height and aspect ratio in plan and height. The elastic properties of the isolation system were lumped at the isolation interface by assuming circular elastomeric devices connected to the nodes of a regular grid at the base. The energy dissipation of the isolation devices was incorporated by assigning a constant damping ratio to the six degrees of freedom of the model. The results of this linear elastic model help identify problems of rocking at the base and tensile loads on the isolators in some cases. The results obtained from the rigid body model for the building were extended to a second parametric model that considers finite stiffness on the superstructure. For the sake of simplicity, 2D non-linear analyses were performed with focus on the isolator tensile loads and the building inter-story drifts. Two building models were considered, a simple frame with three column axes, and a mixed frame with a central wall. The Koh & Kelly non-linear two-spring model was used to characterize the isolators. The results of this analysis show that it is possible to implement seismic isolation in buildings with height-to-base aspect ratio of up to 6:1 without excessive tensile loads on the isolators if theoretical isolation periods go over 6s. Additionally, in these tall and slender buildings, the inter-story displacement reductions decrease with aspect ratio. Also, base shear and floor accelerations are reduced in tall and slender buildings, but the reduction is less significant than the reduction obtained for the relative lateral displacement and drifts.

Keywords: tall isolated buildings, axial-lateral coupling, non-linear parametric analysis, tension on isolators, isolation rocking

1. Introduction

Chile is a highly seismic country, it has three major earthquakes: 1960, Valdivia (Mw=9.5); 1868, Arica (Mw=9.0) and 2010, Maule (Mw=8.8). They correspond to the first, sixth and eighth earthquakes of highest magnitude recorded worldwide [1]. Earthquakes has the potential to make buildings to collapse, causing human and material lost. Because of this, seismic design and protection design techniques are a very relevant issue in the engineering practice in any seismic countries like Chile.

One of the most efficient technique to protect structures of earthquake effects is seismic isolation. This technology has been used with success mostly in low and moderate-rise buildings [2]. The growth and increase in population density in metropolitan areas with the consequent increase in the number of high-rise buildings poses a challenge to seismic isolation. Meanwhile in low rise structures, seismic isolation can reduce the acceleration of floors in one order of magnitude [3], the same could not occur in tall buildings. The slenderness of the building generates a growth in the overturning moment, increasing the possibility of tensile axial loads on isolator devices [4]. Slenderness also generates an increasing of the natural period of the building. It increases the relative displacement between floors, making the decoupling in frequency difficult, which is desirable when isolation is implemented, reducing the beneficial effect of this technology in decreasing floor accelerations [5].

The aim of this research is to explore the implementation of seismic isolation in medium and tall buildings in simple structural models, in order to determine if there is a benefit in using that technology. To achieve this, a parametric analysis was performed using first a simplified representation of the superstructure as a 3D rigid rectangular prism. The results obtained using the above model were extended to a second parametric model that

considers finite stiffness on the superstructure. For the sake of simplicity, 2D non-linear analyses were performed with focus on the isolator tensile loads and the building inter-story drifts. The results of this analysis show that it is possible to implement seismic isolation in buildings with height-to-base aspect ratio of up to 6:1 without excessive tensile loads on the isolators if isolation periods grow over 7s. In tall buildings, the benefit of using seismic isolation lies mainly in reducing the lateral displacements of floor and drifts, resulting in a reduction in the damage on the superstructure. The reduction in the base shear load due to the use of seismic isolation is lower than the reduction in displacement when the building becomes high and slender.

2. Parametric Model of an Isolated Building

2.1. Prismatic 3D Rigid Body Building

In this section, the building was considered as a prismatic rectangular rigid body, geometrically characterized by its height, H, the aspect ratio in plan, $\alpha_1=b/a$, and the slenderness in height, $\alpha_2=H/a$. The dynamic parameters of the building are defined by their mass, m, and the location of its center of mass (x_m,y_m,z_m), as illustrated in Fig. 1.

The isolation system was modeled as a discrete distribution of isolators equally spaced in a rectangular grid. The parametrization of that grid started by defining the number of isolators in the short direction, n_x, then, the number of isolator in the long direction, n_y. Then, it is given by $n_y=1+(n_x-1)\alpha_1$. The elastic properties were defined by the density of rubber area on the plan, ρ_r, the frequency of lateral isolated vibration, ω_I, and the shape factor of the isolator devices, S. The energy dissipation is considered by a constant damping ratio, ξ_I, equal for all 6 modes.

For the sake of simplicity, the asymmetric behavior of the isolated system was considered throught the eccentric location of the mass in the Y direction, by a dimensionless parameter β_2. That is: $y_m=\beta_2 b=H\beta_2\alpha_1/\alpha_2$.

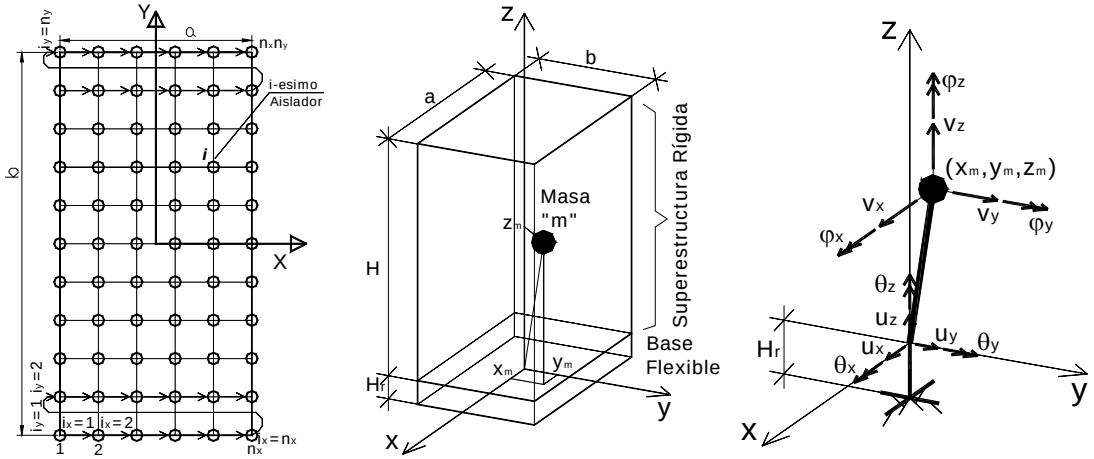

Fig. 1 - Parametrization. (a) Plan of the building with the grid of isolators, (b) Prismatic building, mass and its location, (c) Definition of the 6 d.o.f. at the center of mass, and at the center of stiffness of the isolation level.

2.1.1 Kinematics

In order to define the differential equation that rules the behavior of the system, it is necessary to know the mass, stiffness and damping matrices. All of this matrixes must be related to the vector of degree of freedom (d.o.f.) $\boldsymbol{v}=[v_x, v_y, v_z, \varphi_x, \varphi_y, \varphi_z]^T$, located at the center of mass of the building (Fig. 1(c)).

The kinematic relationship between the d.o.f. of each isolator, $\boldsymbol{u_a}$ (3 displacement for each isolator), and the d.o.f. $\boldsymbol{u}=[u_x, u_y, u_z, \theta_x, \theta_y, \theta_z]^T$ regarding to the centroid of area of the level of isolation (Fig. 1(c)) is given as.

$$\boldsymbol{u_I}=\left[\boldsymbol{u}_I^{(1)},\dots\boldsymbol{u}_I^{(i)},\dots\boldsymbol{u}_I^{(n_xn_y)}\right]^T,\quad \boldsymbol{u}_I^{(i)}=\left[u_x^{(i)},u_y^{(i)},u_z^{(i)}\right]^T=\boldsymbol{L}_i\boldsymbol{u},\quad \boldsymbol{u_I}=\boldsymbol{L_I}\boldsymbol{u},\quad \boldsymbol{L_I}=\left[\boldsymbol{L}_1^T,\dots\boldsymbol{L}_i^T,\dots\boldsymbol{L}_{n_xn_y}^T\right]^T \quad (1)$$

By analyzing Fig 1(c), the kinematic relationship between $\boldsymbol{u}$ and $\boldsymbol{v}$ is given as:

$$\boldsymbol{u}=\boldsymbol{L_u v},\quad \boldsymbol{L_u}=\begin{bmatrix}\boldsymbol{I} & \boldsymbol{Z}\\ \boldsymbol{0} & \boldsymbol{I}\end{bmatrix},\quad \boldsymbol{Z}=\begin{bmatrix}0 & -z_m & y_m\\ z_m & 0 & -x_m\\ -y_m & x_m & 0\end{bmatrix}=\widehat{\boldsymbol{Z}}\boldsymbol{H},\quad \widehat{\boldsymbol{Z}}=\begin{bmatrix}0 & -1/2 & \beta_2\alpha_1/\alpha_2\\ 1/2 & 0 & 0\\ -\beta_2\alpha_1/\alpha_2 & 0 & 0\end{bmatrix} \tag{2}$$

2.1.2 Stiffness Matrix

The stiffness matrix of each isolator, $\boldsymbol{k_I}$, has been considered the same. Then, using the kinematics defined above, the stiffness matrix, $\boldsymbol{K}$, of the isolated building relative to the d.o.f. at its center of mass is determined as

$$\boldsymbol{K}=\boldsymbol{L_u^T K_u L_u},\quad \boldsymbol{K_u}=\boldsymbol{L_I^T K_I L_I},\quad \boldsymbol{K_I}=\begin{bmatrix}\boldsymbol{k_I} & \dots & \boldsymbol{0}\\ \vdots & \ddots & \vdots\\ \boldsymbol{0} & \dots & \boldsymbol{k_I}\end{bmatrix},\quad \boldsymbol{k_I}=\begin{bmatrix}k_x & 0 & 0\\ 0 & k_y & 0\\ 0 & 0 & k_z\end{bmatrix},\quad \begin{matrix}k_x=k_y=k_h\\ k_z=\frac{E_c}{G}k_h\end{matrix} \tag{3}$$

where E_c is the effective modulus of elasticity of a single rubber layer under axial load, G is the shear modulus of the rubber, and k_h is the horizontal stiffness of a single isolator, considering opposite faces remain horizontal. In the stiffness $\boldsymbol{k_I}$, the axial lateral coupling was neglected, and the rubber was assumed as a perfectly incompressible material, then, $E_c=6GS^2$, in the case of a circular isolator used in the analysis.

The horizontal stiffness of the isolated building, K_h, is defined from the parameters of the model as

$$K_h=m\omega_I^2=n_xn_yk_h,\ \ k_h=\frac{GA}{H_r},\ \ A=\frac{\rho_r ab}{n_xn_y},\ \ \left\{\begin{matrix}a=H/\alpha_2\\ b=\alpha_1H/\alpha_2\end{matrix}\right\},\ \ =>\ K_h=\frac{G\rho_r\alpha_1H^2}{{\alpha_2}^2H_r} \tag{4}$$

2.1.3 Mass Matrix

As a basic assumption, it was considered that the mass is distributed in the volume of the prismatic building. Within it, the density of mass has not variation in the X and Z directions, and has linear variation in the Y direction. Considering the above, the rotational inertias of mass, I_x, I_y and I_z, around the X, Y, and Z axes were defined as:

$$I_i=mH^2\hat{I}_i,\ \ i=x,y,z;\quad \hat{I}_x=\frac{1}{12}\left(1+(1-12{\beta_y}^2)\left(\frac{\alpha p}{\alpha_h}\right)^2\right);\quad \hat{I}_y=\frac{1}{12}\left(1+\left(\frac{1}{\alpha_h}\right)^2\right);\quad \hat{I}_z=\frac{1}{12}\left(\left(\frac{\alpha p}{\alpha_h}\right)^2+\left(\frac{1}{\alpha_h}\right)^2\right) \tag{5}$$

And the matrix of mass, referred to the d.o.f. $\boldsymbol{v}=[v_x, v_y, v_z, \varphi_x, \varphi_y, \varphi_z]^T$, is given as:

$$\boldsymbol{M}=m\widehat{\boldsymbol{M}};\quad \widehat{\boldsymbol{M}}=\begin{bmatrix}\boldsymbol{I} & \boldsymbol{0}\\ \boldsymbol{0} & \widehat{\boldsymbol{M}}_2H^2\end{bmatrix};\quad \widehat{\boldsymbol{M}}_2=\begin{bmatrix}\hat{I}_x & 0 & 0\\ 0 & \hat{I}_y & 0\\ 0 & 0 & \hat{I}_z\end{bmatrix} \tag{6}$$

2.1.4 Damping Matrix

This matrix was defined from a constant ratio of critical damping, ξ_I, for all 6 modes. In order to determine the damping matrix, the problem of eigenvalues and eigenvectors must be solved first.

$$[\boldsymbol{K}-{\omega_n}^2\boldsymbol{M}]\boldsymbol{\phi}_n=0;\quad but, \boldsymbol{K}=m\omega_I^2\widehat{\boldsymbol{K}},\ \ defining\ \ \widehat{\omega}_n=\omega_n/\omega_I,\ \ then: \left[\widehat{\boldsymbol{K}}-{\widehat{\omega}_n}^2\widehat{\boldsymbol{M}}\right]\boldsymbol{\phi}_n=0 \tag{7}$$

Then, the normalized matrix of natural frequencies, $\widehat{\boldsymbol{\Omega}}$, and the matrix of eigenvectors, $\boldsymbol{\Phi}$, can be obtained as:

$$\widehat{\boldsymbol{\Omega}}=\begin{bmatrix}\widehat{\omega}_1 & \dots & 0\\ \vdots & \ddots & \vdots\\ 0 & \dots & \widehat{\omega}_6\end{bmatrix};\quad \boldsymbol{\Omega}=\omega_I\widehat{\boldsymbol{\Omega}};\quad \Phi=[\boldsymbol{\phi}_1\ \ \dots\ \ \boldsymbol{\phi}_6];\quad satisfying\ that:\ \Phi^{\boldsymbol{T}}\widehat{\boldsymbol{M}}\Phi=\boldsymbol{I},\ \text{and}\ \ \Phi^{\boldsymbol{T}}\widehat{\boldsymbol{K}}\Phi=\widehat{\boldsymbol{\Omega}}^{\boldsymbol{2}} \tag{8}$$

Using the above matrixes, the damping matrix can be determined as:

$$\boldsymbol{C}=\Phi^{-\boldsymbol{T}}\widehat{\boldsymbol{C}}\Phi^{-\boldsymbol{1}};\quad \widehat{\boldsymbol{C}}=2\xi_I\omega_I\widehat{\boldsymbol{\Omega}} \tag{9}$$

2.1.5 Dynamic Equilibrium

The differential equation that rules the behavior of the isolated rigid body building is given as:

$$\boldsymbol{M\ddot{v}}+\boldsymbol{C\dot{v}}+\boldsymbol{Kv}=-\boldsymbol{Mr_g\ddot{u}_g};\quad \boldsymbol{v}(t=0)=\boldsymbol{v_0};\quad \dot{\boldsymbol{v}}(t=0)=\dot{\boldsymbol{v}}_{\boldsymbol{0}} \tag{10}$$

where r_g is a kinematic matrix of influence of the earthquake $\ddot{u}_g$ on the d.o.f. $\boldsymbol{v}$, of the isolated system.

$$\boldsymbol{r_g} = [\boldsymbol{I} \quad \boldsymbol{0}]^T; \quad \ddot{\boldsymbol{u}}_{\boldsymbol{g}} = \left[\ddot{u}_{gx}^T \quad \ddot{u}_{gy}^T \quad \ddot{u}_{gz}^T\right]^T \tag{11}$$

Due to the acceleration of gravity, g, was not included in the component Z of the ground acceleration, the initial condition of the differential equation are homogeneous. Because of this, in the calculations of the normal stress on isolators, the static load must be added to the dynamic axial load.

2.2. Flexible Frame as a 2D Model

Even though the results obtained with the above formulation can provide a good approximation of the lateral displacements, the same could not occur for axial loads on isolators. The last is because the structure is actually much more stiff laterally than the isolation system, but the vertical stiffness of isolators are of the same order of magnitude as the elements of the superstructure that resist vertical loads. Due to the above, and to better identify the problems of rocking at the base and tensile loads on the isolators, a second model that incorporate the stiffness of the superstructure and the nonlinear behavior of the rubber bearings was developed. In this model, and only for simplicity, the structure was assumed as a 2D flexible frame, eliminating the parameter "eccentricity of mass" from the model. The cross sections of columns and beams are equal in blocks of 5 storeys, as shown in Table 1.

In the model used for the superstructure, columns and beams were considered axially very stiff, including a horizontally rigid diaphragm on each floor. The cross sections of columns and beams are equal in blocks of 5 storeys, bein the smaller cross section at the five higher storeys and growing down, as shown in Table 1.

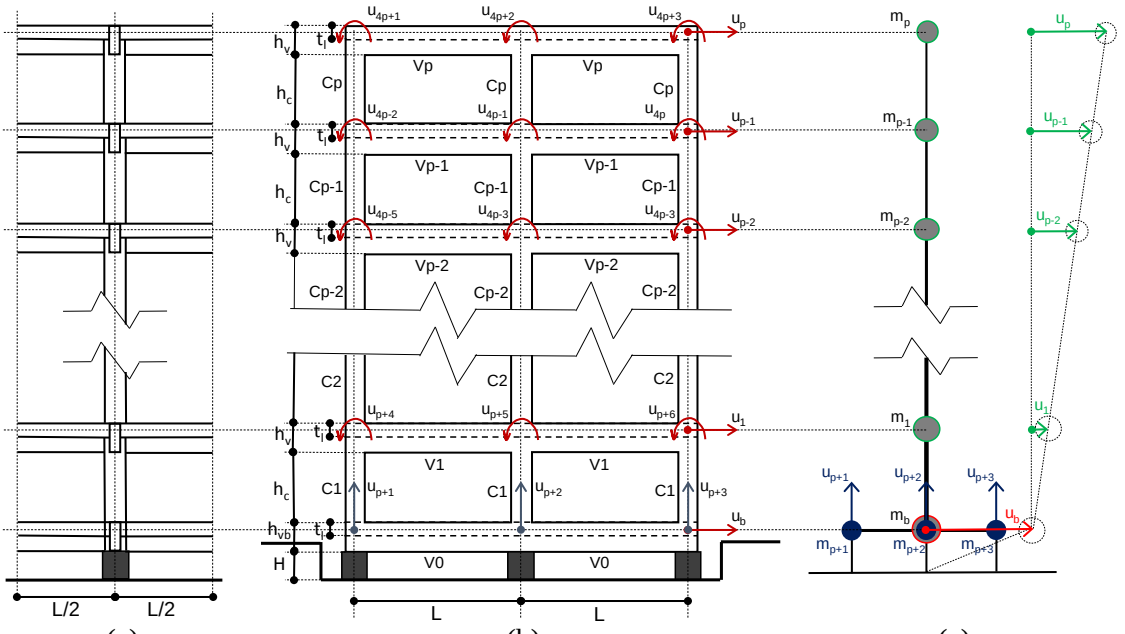

Fig. 2 - Scheme of the structure. (a) Tributary width and section. (b) Elevation of the frame and d.o.f. before condensation. (c) Condensed d.o.f. and masses of the isolated structural model

2.2.1 Mass, Stiffness and Damping in Superstructure

After assembling the stiffness matrix of the superstructure according the d.o.f. in Fig 2(b), this matrix was condensed to the lateral and vertical displacements of the base, as shown in Fig. 2(c). The mass matrix is diagonal, and referred to the d.o.f. of Fig. 2(c), being the mass determined by tributary volumes. The mass and stiffness matrices above, are then restricted laterally in the base (d.o.f. u_b in Fig 2(c)), obtaining the matrices $\boldsymbol{M_s}$ and $\boldsymbol{K_s}$ respectively. The mass related to the lateral d.o.f. u_b, denoted m_b, is determined as the tributary mass of the level of isolation, and this mass is not included in $\boldsymbol{M_s}$ after it is linked at the base.

In order to consider the energy dissipation on the superstructure, a constant rate of the critical damping, ξ_s, was considered for all modes. The damping matrix $\boldsymbol{C_s}$ was calculated from the eigenvalue and eigenvectors of the

superstructure, and a constant damping ratio ξ_s. However, because the stiffness matrix $\boldsymbol{K_s}$ is singular, only for determining the damping matrix $\boldsymbol{C_s}$, the stiffness matrix $\boldsymbol{K_{sv}}$ —linked vertically in the base by flexible elements— was defined. The stiffness of the vertical links was considered equal to the vertical stiffness of the isolators under null lateral displacement. Then, the eigen-problem to solve and the damping matrix are given by

$$[\boldsymbol{K_{sv}} - \omega_n{}^2 \boldsymbol{M_s}]\boldsymbol{\phi}_n = 0; \quad n = 1, 2, \ldots p+3; \quad \boldsymbol{\Omega_s} = \begin{bmatrix} \omega_1 & \ldots & 0 \\ \vdots & \ddots & \vdots \\ 0 & \ldots & \omega_{p+3} \end{bmatrix}; \quad \Phi_s = [\boldsymbol{\phi}_1 \quad \ldots \quad \boldsymbol{\phi}_{p+3}]; \tag{12}$$

$$\boldsymbol{C_s} = \Phi_s^{-T} 2\xi_s \boldsymbol{\Omega_s} \Phi_s^{-1}; \quad satisfaing\ that: \Phi_s^T \boldsymbol{M_s} \Phi_s = \boldsymbol{I}; \ \Phi_s^T \boldsymbol{K_{sv}} \Phi_s = \boldsymbol{\Omega_s^2} \tag{13}$$

2.2.2 Dynamic Equilibrium

The formulation of the dynamic equilibrium equation of the isolated system, considers that lateral and vertical displacement of the isolation level (u_b and $\boldsymbol{u}_v$=[u_{p+1}, u_{p+2}, u_{p+3}]^T in Fig 2(c)) are relative to the ground, and lateral displacement of floors (u_1, u_2,… u_p in Fig. 2(c)) are relative to the base. In the equilibrium, forces acting on the lateral and vertical d.o.f. of the isolation level, u_b and u_v, are nonlinear from the isolation system. This nonlinearity considers the nonlinear elastic behavior including axial lateral coupling, and the nonlinear plastic behavior due to the rubber internal damping. The first one was characterized by using the two-springs model [6], and its modifications [7], and the second one by using the elastic-plastic Bouc-Wen differential equation, adapted for isolation devices [8]. Then, the equilibrium leads to:

$$\begin{bmatrix} m_b + \boldsymbol{r}_b^T \boldsymbol{M_s} \boldsymbol{r}_b & \boldsymbol{r}_b^T \boldsymbol{M_s} \\ \boldsymbol{M_s} \boldsymbol{r}_b & \boldsymbol{M_s} \end{bmatrix} \begin{bmatrix} \ddot{u}_b \\ \ddot{\boldsymbol{u}}_s \end{bmatrix} + \begin{bmatrix} 0 & \boldsymbol{0} \\ \boldsymbol{0} & \boldsymbol{C_s} \end{bmatrix} \begin{bmatrix} \dot{u}_b \\ \dot{\boldsymbol{u}}_s \end{bmatrix} + \begin{bmatrix} 0 & \boldsymbol{0} \\ \boldsymbol{0} & \boldsymbol{K_s} \end{bmatrix} \begin{bmatrix} u_b \\ \boldsymbol{u}_s \end{bmatrix} + \begin{bmatrix} f_b(u_b, z) \\ \boldsymbol{F_s}(\boldsymbol{u_v}) \end{bmatrix} = -\begin{bmatrix} m_b + \boldsymbol{r}_b^T \boldsymbol{M_s} \boldsymbol{r}_b \\ \boldsymbol{M_s} \boldsymbol{r}_b \end{bmatrix} \boldsymbol{r}_g \ddot{\boldsymbol{u}}_g \tag{14}$$

$$\dot{z} = \frac{\dot{\boldsymbol{u}}_b}{\boldsymbol{u_y}} \left(1 - \frac{1}{2}|z|^n \left(1 + sign(diag(\dot{u}_b) z)\right)\right) \tag{15}$$

where $\boldsymbol{r}_b = [1, \ldots 1, 0, 0, 0]^T$ is a $p+3$ by 1 vector and $\boldsymbol{r}_g$=1, and both are kinematics.

In Eq. (14), f_b is the nonlinear base shear force due to the geometric and plastic nonlinear behavior of the isolators. The vector of forces $\boldsymbol{F}_s$ contains the axial forces on each isolator on the base, and they are nonlinear only due to the geometrical axial-lateral coupling.

2.3. Frame with Central Wall as a 2D Model

In the analysis of a seismically isolated frame, the maximum axial loads occurs at the external isolators, and this load does not have direct correlation with the bending moment in the columns and beams supported on those isolators, but mainly with the axial loads in the column. In this model, a wall is included at the center of the structure (Fig. 3), having this wall the higher contribution to the lateral stiffness of the superstructure.

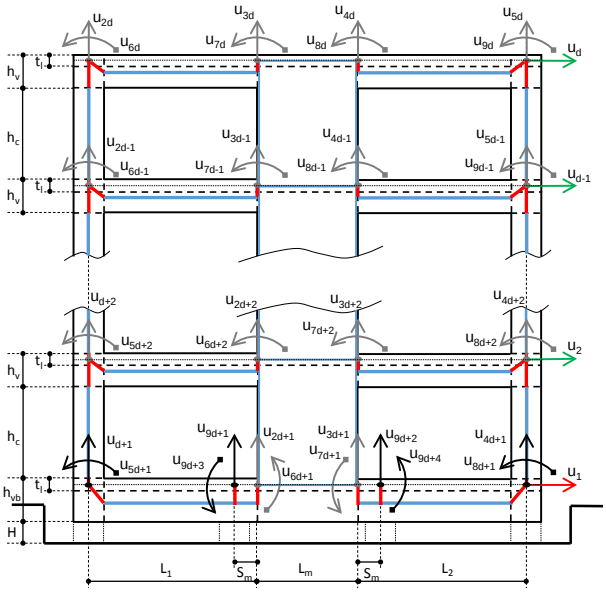

Fig. 3 - Scheme of the super-structure with all the d.o.f. and the location of isolators in base by doted lines.

At the base of the structure, there are four equal circular isolators, among which two are located below the columns, and two at the interior, near or just below the ends of the central wall (Fig. 3).

In the model used for the superstructure, columns were considered axially flexible, but beams were considered axially very stiff, because the inclusion of a horizontally rigid diaphragm on each floor. Then, the columns were modeled using an Euler-Bernoulli element of 6 d.o.f., and beams by a 4 d.o.f. element. The walls were modeled using a single rectangular element of 3 d.o.f for each node (two displacement and one rotation). A single element was used for modeling the wall at each floor. The cross sections of columns and beams and the width of the walls are equal in blocks of 5 storeys, being the smaller cross section at the five higher storeys and growing down.

2.3.1 Mass, Stiffness and Damping in Superstructure

Before formulating the equation of equilibrium, the stiffness matrix of the superstructure related to the d.o.f. of Fig. 3 must be condensed to the lateral and vertical displacements of the floors, plus the rotations on the base at the locations of the isolators. This mass matrix is diagonal, and it is referred to the same d.o.f. of the above condensed stiffness matrix, being the masses determined by tributary volumes. From here, the procedure to be followed is similar to that indicated in *2.2.1*, leading to the matrixes $\boldsymbol{M_s}$ and $\boldsymbol{K_s}$, $\boldsymbol{K_{sv}}$ and finally $\boldsymbol{C_s}$ from a constant rate of critical damping, ξ_s, for all modes, by solving the eigenproblem between $\boldsymbol{K_{sv}}$ and $\boldsymbol{M_s}$.

For simplicity, the distance S_m in Fig. 3 was set to zero, then the length of the wall, L_m, is the same to the distance between the edges of the wall to the axis of the adjacent column, L. The above, eliminates the d.o.f. d+1 to d+4 —where d is the number of diaphragm of floors— and locating the central isolators just above the ends of the wall.

2.3.2 Dynamic Equilibrium

The formulation of the dynamic equilibrium equation is similar to that presented in *2.2.2*, but in this case, the vertical d.o.f. were conserved in all floors. This is because the formulation of the wall need the vertical displacement at the 4 corners to the element to reproduce correctly his lateral and flexural stiffness. Because of the above, and the fact that in this model there are 4 —and not 3— isolator in the base, the kinematic $\boldsymbol{r}_b$ is not the same defined in *2.2.2.* Here, the kinematic is a *1* by *5(d-1)* vector, with *d-1* ones follow by *4(d-1)* zeros given as $\boldsymbol{r}_b = [1, \dots 1, 0, \dots, 0]^T$, where d is the number of rigid diaphragms of floor.

3. Results of the Analysis

In all the formulations described above, the input of the analysis is a seismic record. In the present paper, the N60ºE seismic record on February 27th of 2010 at Concepción station, was used as input. In order to be consistent with the requirement of the Chilean code for seismic isolated structures, NCh2745 [9], the seismic record was modified in the frequency domain to adjust its response spectrum to the design spectrum of the normative. The horizontal input acting in the weak direction of the structure was compatibilized with the spectrum of design of this code. This means that the seismic record is modified in the frequency domain, seeking as aim to match the spectrum of elastic response of the modified seismic record, with the seismic design spectrum of the code. The seismic input in the strong direction of the structure —in the case of the 3D model— or out of the plane of analysis —in the case of 2D models— has been considered null. The vertical seismic input has been considered in all cases of analysis, equal to the seismic record, without any modification.

In sections 3.2 and 3.3, the superstructure was considered made of reinforced concrete, using an elasticity modulus $E=2\cdot10^5$ kg/cm^2 for this material.

3.1. Prismatic 3D Rigid Body Building

After obtaining the response of the 3D rigid isolated building for all combinations of the parameters considered, the maximum responses of base horizontal displacement, base absolute acceleration and normal average stress

on isolator were determined for all the duration of the seismic input. Then, the maximum absolute of this responses were obtained for any analysis performed, taking out the time as a variable. The above results are shown in Figs. 4 to 8.

By analyzing Figs. 4 to 7, it is observed that the maximum lateral displacement and absolute acceleration of the base do not depend on the slenderness of the building, α_2, if the shape factor is high enough.

In Fig. 8, the maximum average stress, normalized to the static stress, $\sigma_z^{norm}=(P_z^{max}/A)/\sigma_z^{static}$ is shown. In the last definition, the stress σ_z^{static} is the average stress due to static weight. In Fig. 8, where all curves for different rates of aspect of the plan α_2, are shown. It is possible to observe that the parameters α_2 and S, have little influence on the maximum stress on the isolators, when the building is very stiff.

From Figs. 4 to 8, it is possible to observe that the eccentricity of mass, β_2, has direct influence on the maximum lateral displacement and absolute acceleration of the base, and also on the maximum compressive and tensile stress on isolators.

If there is eccentricity of mass, an increasing of the aspect ratio, α_2, causes an increase in the maximum displacement and maximum acceleration of the base.

In general, regarding to normal tensile stresses on isolators, it was observed that this is reduced with the lengthening of the isolation period. It is found that, even in cases with mass eccentricity of 10% and high slenderness of 8:1, it is possible to eliminate the tractions on isolators for long periods higher than 6 seconds.

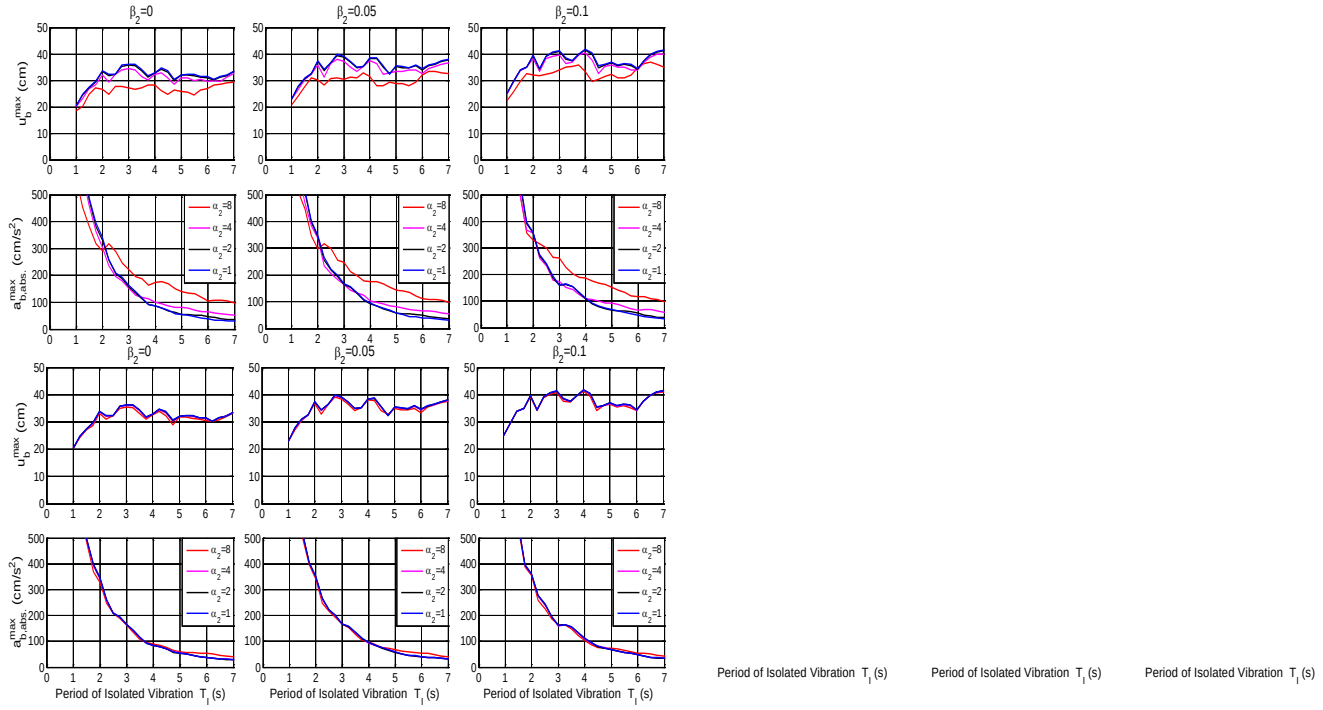

(a) (b)

Fig. 4 - Maximum responses of base. (a) α_1=1, ξ_b=10% and S=10. (b) α_1=1, ξ_b=10% and S=30

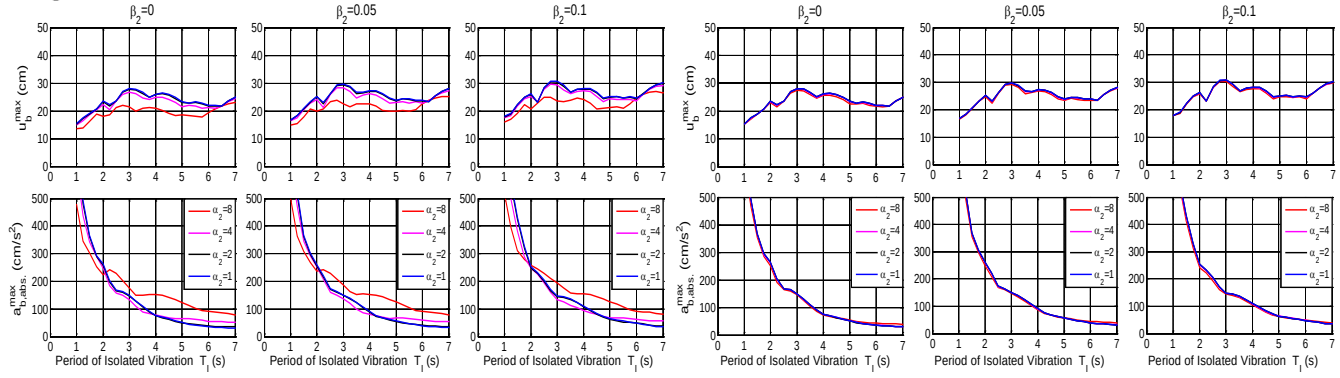

(a) (b)

Fig. 5 - Maximum responses of base. (a) α_1=1, ξ_b=20% and S=10. (b) α_1=1, ξ_b=20% and S=30

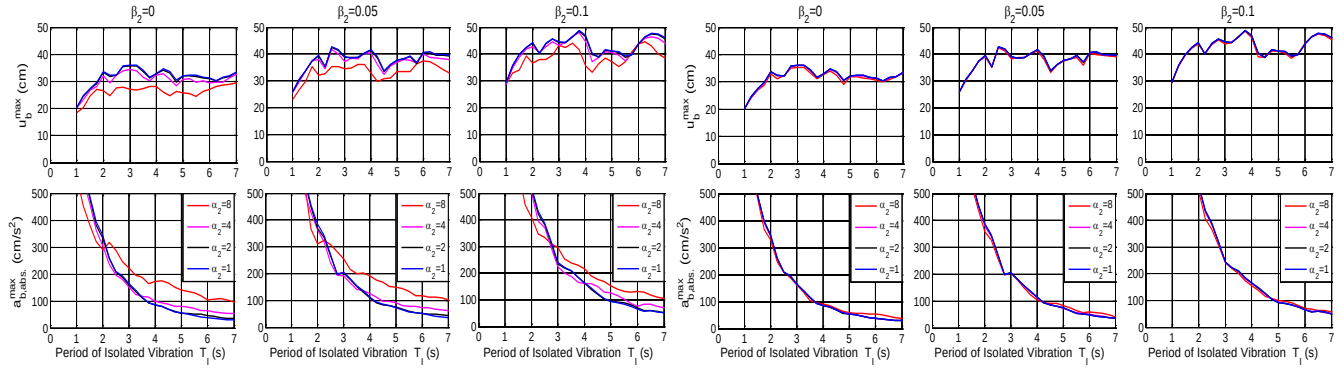

(a) (b)

Fig. 6 - Maximum responses of base. (a) α_1=3, ξ_b=10% and S=10. (b) α_1=3, ξ_b=10% and S=30

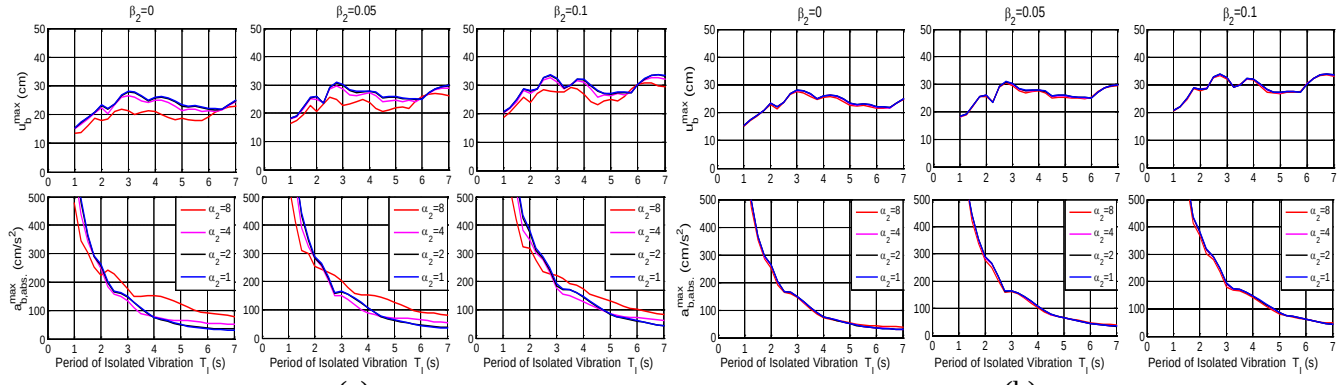

(a) (b)

Fig. 7 - Maximum responses of base. (a) α_1=3, ξ_b=20% and S=10. (b) α_1=3, ξ_b=20% and S=30

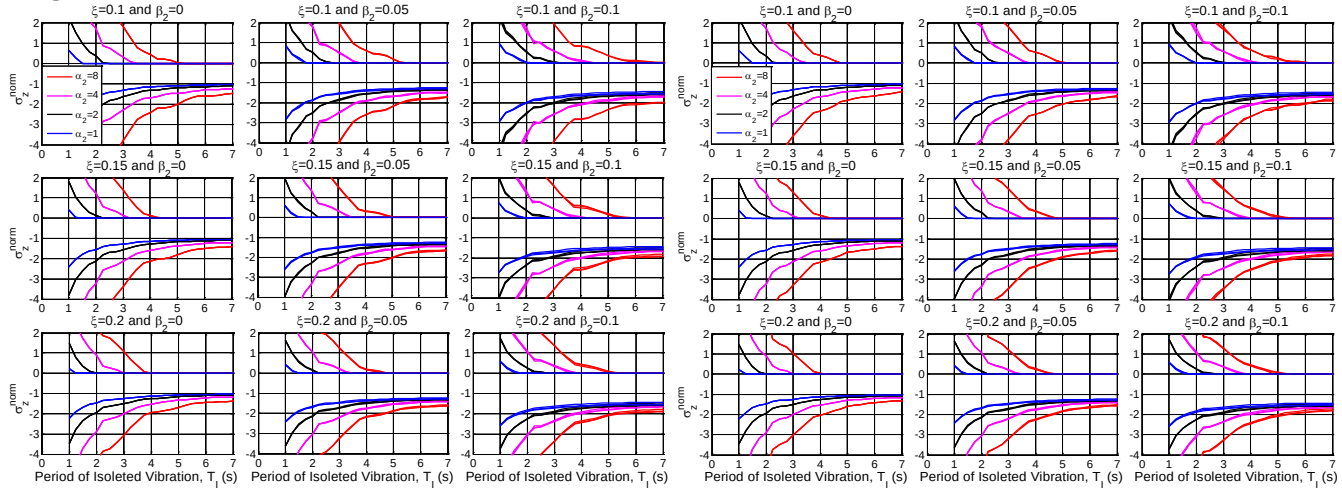

(a) (b)

Fig. 8 - Max. normalized axial stress on isolators for α_1=1, 2, 3 superposed. (a) S=10. (b) S=30. Curves below the period axis (negative stress) are compression, and above that axis (positive stress), are tension.

3.2. Flexible Frame as a 2D Model

This analysis seeks to verify the results obtained in the previous section in a more realistic way, by incorporating flexibility in the superstructure and a nonlinear behavior of the isolators. To achieve this, and only to reduce the number of parameters, the damping in the superstructure was considered ξ_s=2% of the critical and at the interface of isolation it was taken equal to ξ_b=10% of the critical, for all the analysis performed in this section.

The properties of the superstructure and base isolation system are shown below. The height between floors is 2.65m, and L=6m (Fig. 2). In Figs. 9 and 10, the maximum responses of the analyses performed are shown.

Table 1: Cross section of columns and beams for each block of floors. N is the number of storeys from 1 to 30.

Floors	N-4→N	N-9→N-5	N-14→N-10	N-19→N-15	N-24→N-20	N-29→N-25	Base
h_b (cm)	60	60	60	60	60	60	100
t_b (cm)	15	20	25	30	35	40	45
b_c (cm)	30	35	40	45	50	55	60

Table 2: Parameters of design of the isolation system, as a function of the number of storeys of the frame.

N storeys	2	4	6	8	10	12	14	16	18	20	22	24	26	28	30
D_{iso} (cm)	30	34	40	46	51	55	60	64	69	72	76	80	84	88	91
H_r (cm)	12.9	10	10	10	10	14.7	21.1	28.6	37.5	47.9	59.5	70.9	83.8	83.8	83.8
T_{fix} (s)	0.15	0.31	0.48	0.66	0.85	1.05	1.25	1.46	1.68	1.89	2.11	2.33	2.54	2.75	2.96
T_{iso} (s)	2.5	2.5	2.5	2.5	2.55	3.14	3.76	4.38	5.02	5.67	6.32	6.97	7.5	7.5	7.5
α_2 Slenderness	0.38	0.77	1.14	1.51	1.89	2.27	2.65	3.03	3.41	3.79	4.16	4.54	4.92	5.3	5.67

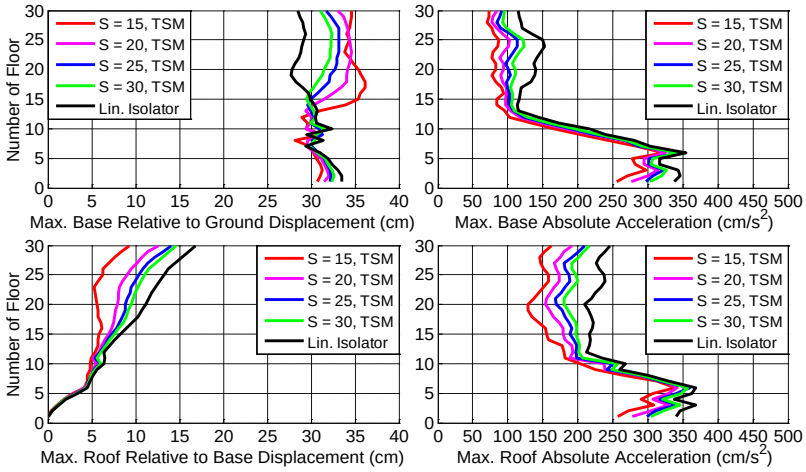

Fig. 9 - Max. response of the isolated system, using the Two-Springs-Model (TSM) and linear model for isolators

(a) (b) (c)

Fig. 10 - Axial response of isolators (a) Load P, for S=15. (b) Load P, for S=30 (c) Max. average stress P/A.

By observing Fig. 9, the responses of the system using the Two-Springs-Model (TSM) [6, 7] and a Linear model for the isolators tend to be closer when the shape factor S grows. This is explained because the geometric nonlinearity characterize by using the TSM is negligible when shape factor grows. In the latter case, the differences observed correspond to the way of characterizing the energy dissipation. In the linear model the dissipation is considered by a viscous damping and in the non-linear model it is added by an equivalent hysteretic damping.

Unlike the observed from the results of the rigid building model, in this analysis the shape factor S does have influences in the maximum axial stress reached on the insulators. By including the flexibility of the superstructure, higher axial stresses on the isolators are observed when the shape factor grows. However, in none of the cases analyzed tensile loads on isolators were observed.

3.3. Frame with Central Wall as a 2D Model

This analysis corresponds to the more realistic model analysed herein. Its aim is to confirm the results obtained in the previous section and evaluate the effect of including a wall and different periods of isolation in the response of the system. In the analysis performed, the damping in the superstructure was considered ξ_s=2% of critical damping.

The height between floors is 2.65m, and L=L_m=6m (Fig. 3). Then, the slenderness for buildings of 10, 20, 30 and 40 storeys are α_2=1.47, 2.94, 4.41 and 5.89 respectively. The properties of the structure and isolation system are shown below. In Figs. 11 to 17, the maximum responses are shown, for buildings of 10, 20, 30 and 40 storeys.

Table 3: Parameters of design of the isolation system for short and long isolation periods

	Short Isolation Periods	**Long Isolation Periods**

Nº Storeys	T_{fix} (s)	ξ_b (%)	D_{iso}(cm)	H_r (cm)	T_{iso} (s)	S	D_{iso}(cm)	H_r (cm)	T_{iso} (s)	S
10	0.58	5:5:20	82	22.0	2.42	10.3	56	33.5	4.51	28.0
20	1.73	5:5:20	96	22.0	2.93	12.0	78	72	6.98	32.5
30	2.92	5:5:20	98	33.6	4.47	20.4	98	88	7.66	30.6
40	3.99	5:5:20	116	61.0	6.01	29.0	116	96.3	7.80	32.2

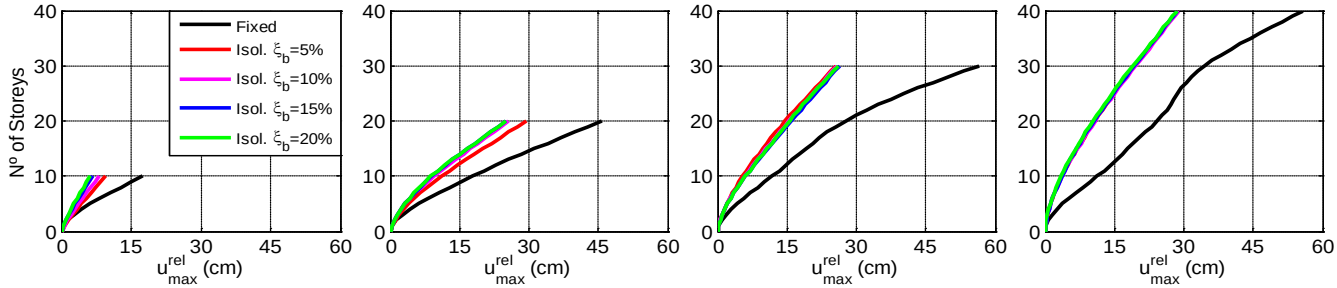

Fig. 11 - Maximum lateral displacement of floor for short isolation periods.

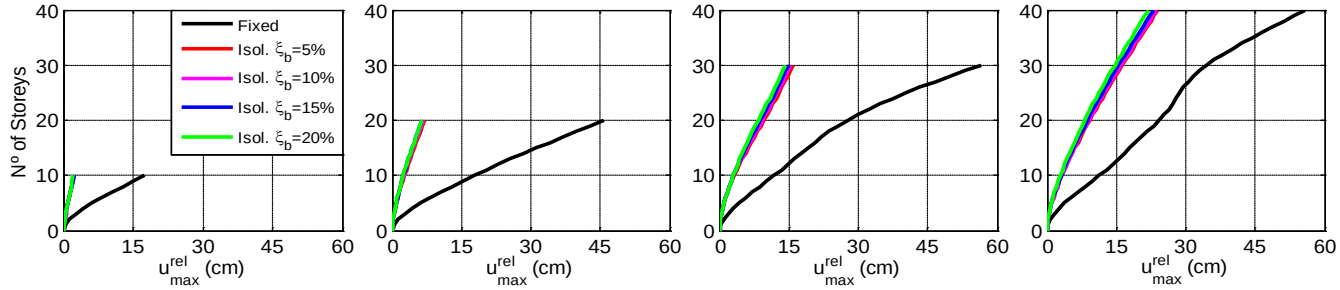

Fig. 12 - Maximum lateral displacement of floor for long isolation periods.

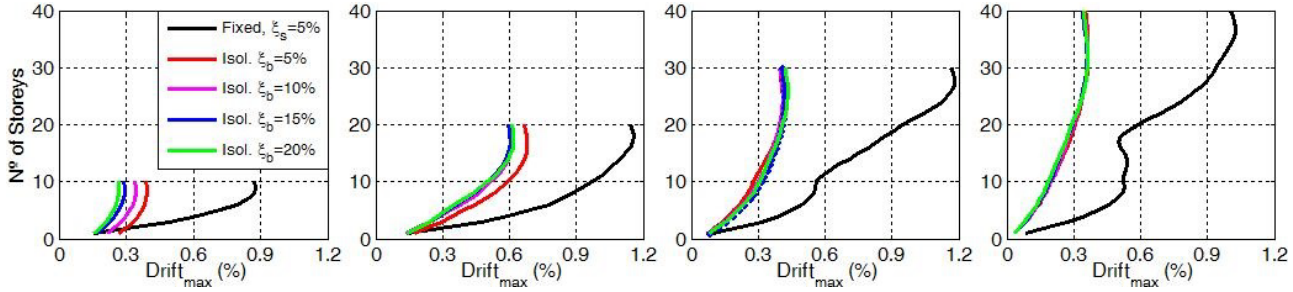

Fig. 13 - Maximum relative displacement between floors, DRIFT, for short isolation periods.

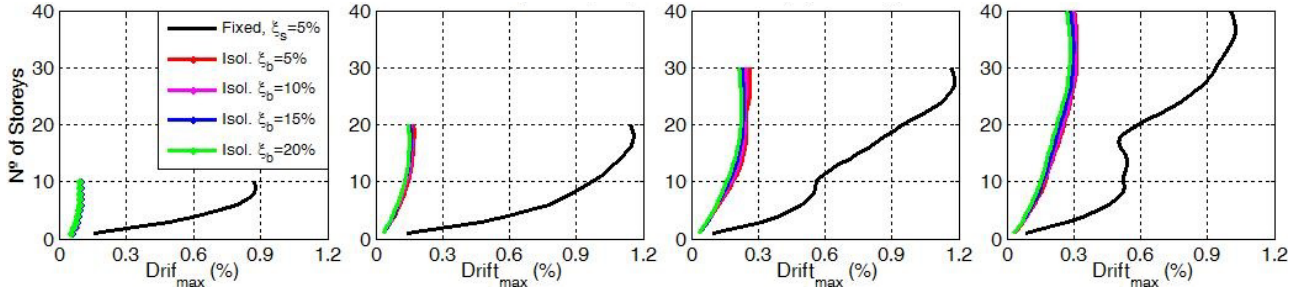

Fig. 14 - Maximum relative displacement between floors, DRIFT, for long isolation periods.

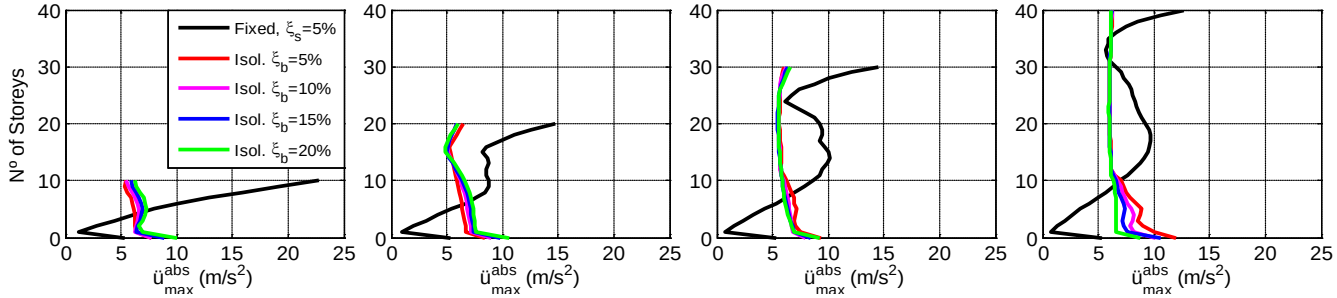

Fig. 15 - Maximum lateral absolute acceleration of floor for short isolation periods.

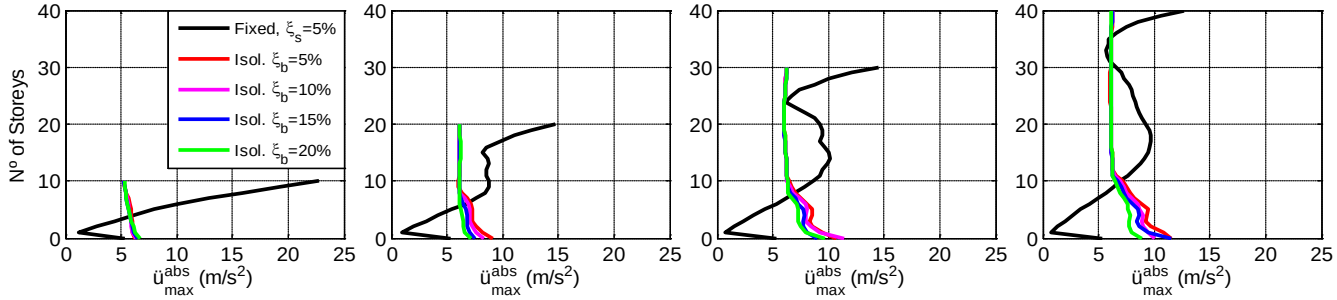

Fig. 16 - Maximum lateral absolute acceleration of floor for long isolation periods.

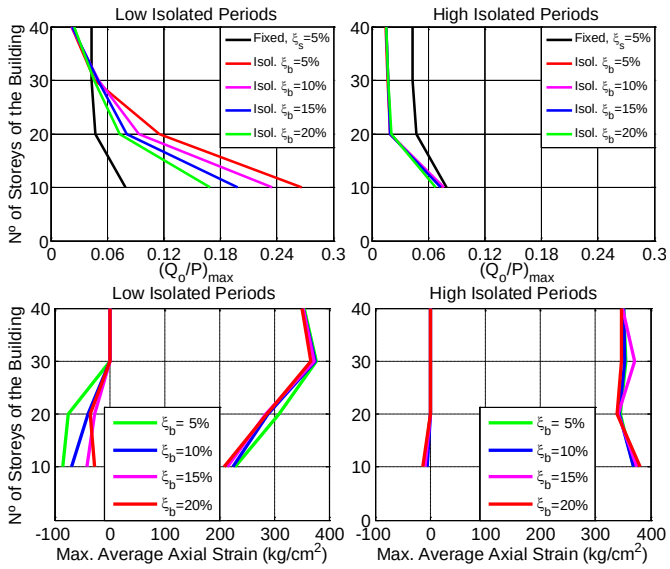

(a) (b)

Fig. 17 - Normalized shear load (a) and maximum average strain on isolators (b) for short and long isolated periods

From Figs. 11 to 14, the benefit of using base isolation with short and long isolated periods is observed in the reduction of the relative lateral displacement of floors and drifts. The base isolation with longer periods shows a more significant benefit for low and compact buildings (10 and 20 storeys) than for tall and slender buildings (30 and 40 storeys). However, from Figs. 15 and 16, it is observed that the benefit of using base isolation in the reduction of absolute accelerations of floors is only achieved for low buildings (10 storeys).

The results shown in Fig. 17(a) indicate the necessity of long periods of isolation for obtaining a reduction in the base shear force. However, for purposes of design, according the Chilean code for seismic isolated buildings [9], the base shear load must not be taking less than a certain threshold. Therefore, base isolation result to be effective in practice to reduce the base shear load only for low rise buildings or medium-low slender buildings. Despite the above, isolation is useful for reducing the relative lateral displacement and drifts in the superstructure, and then, protect it from seismic damage.

The results of Fig. 17(b), shown that tensile load on isolators is a problem for low-rise buildings and/or short isolation periods. In order to protect the isolation devices from the cavitation by tensile stress, a long period of isolation is required not only for medium and high or slender building, but also for low rise and compact buildings.

4. Conclusions

This research studies elastomeric seismic isolation of tall and slender buildings. Its aim is to identify and numerically evaluate the most significant aspect that hinder implementation of this technology in practical structures. In general, results show that it is technically possible to incorporate elastomeric seismic isolation in buildings of slenderness up to 6:1 without isolator tension, and at the same time achieve relevant reduction in inter-story deformations in the superstructure.

Larger plan eccentricities from the center of mass relative to the center of stiffness lead to an increase in lateral displacements, drifts, and total floor accelerations. These tendencies become more evident for larger plan aspect ratios. Furthermore, the response amplification due to an irregular distribution of masses in the superstructure could be reduced by aligning the center of stiffness of the isolation system with the vertical projection of the center of mass of the superstructure.

Because as the building goes taller and more slender, the fundamental building period increases. To decouple isolated and fixed-to-base frequencies it is then necessary to achieve a longer isolation period in order for the isolation to be effective. Results show that the isolation system is very effective in reducing relative displacements, total accelerations, and base shear in low-rise buildings with slenderness smaller than 3. However, as the building grows taller and more slender, the efficiency of the isolation system decreases in terms of the base shear and total accelerations in the superstructure, but remains effective in reducing lateral drifts in the superstructure. These results imply that it is physically feasible to use long period seismic isolation systems for reducing the deformation in the superstructure of tall and slender buildings, thus reducing internal forces and building damage.

5. References

[1] Moreno G, Novoa C (2015): Seis terremotos ocurridos en Chile se ubican entre los 25 más potentes de la historia. (HTML) EMOL.

[2] Kelly, M. and Aiken, Ian D. (1991). “Experimental Studies of the seismic response of structures incorporating base-isolation sistems”, Nuclear Engineering and Design, Vol 27, Issue 3, Vol. 2, pag. 239-338.

[3] Kelly J. M., (1998). “Base Isolation: Origins and Development”, National Information Service for Earthquake Engineering, University of California at Berkeley.

[4] Koichiro, Kimoto (2007). “Progression of Seismic Isolation Design During This 20 Years in Japan”, SAI Structural Co. Ltda.

[5] Kulkarni, Jeevan A. and Jangid, R. S. (2002). “Rigid Body Response of Base-Isolated Structures”, Journal of Structural Countrol, Vol 9, pag. 177-188.

[6] Koh, C. G., & Kelly, J. M. (1988). A simple mechanical model for elastomeric bearings used in base isolation. International journal of mechanical sciences, 30(12), 933-943.

[7] James M. Kelly, 2003. Tension Buckling in multilayer elastomeric bearing. Journals of Engineering Mechanics ASCE, December 2003.

[8] Ismail, M., Ikhouane, F., & Rodellar, J. (2009). The hysteresis Bouc-Wen model, a survey. Archives of Computational Methods in Engineering, 16(2), 161-188.

[9] Norma Chilena Oficial, NCh 2745, Oficial 2003. Análisis y Diseño de Edificios con Aislación Sísmica. Instituto Nacional de Normalización, INN-Chile.